Plasma Physics Reports, Vol. 27, No. 7, 2001, pp. 625–633. Translated from Fizika Plazmy, Vol. 27, No. 7, 2001, pp. 664–672.

LOW-TEMPERATURE PLASMA

Ionization of Sputtered Metal Atoms in a Microwave ECR Plasma Source

N. P. Poluektov, V. N. Kharchenko, and I. G. Usatov

Moscow State University of Forestry, Pervaya Institutskaya ul. 1, Mytishchi, Moscow oblast, 141005 Russia

Received November 29, 2000; in final form, February 2, 2001

Abstract—The ionization of sputtered aluminum atoms in the plasma of a microwave ECR discharge intended for metal coating of submicron-size structures in microelectronics is studied. The spatial distributions of xenon plasma parameters and their variations under the action of metal atoms are investigated using probe and optical emission spectroscopy techniques. © *2001 MAIK "Nauka/Interperiodica".*

1. INTRODUCTION

Present-day ULSI technology requires the metallization of submicron-size vias and trenches with an aspect (depth-to-width) ratio of 2–5. The use of magnetron sputtering for this purpose encounters serious difficulties. The flow of sputtered metal is almost completely atomic. The angular distribution of sputtered atoms is approximately described by a cosine function. When filling high-aspect-ratio submicron structures, this nearly isotropic distribution of metal atoms results in the formation of an overhang at the entrance to the structure and a void inside it. In order for the filling to be conformal, it is necessary that the majority of incident particles be accelerated perpendicular to the substrate surface. The broad angular spectrum of sputtered atoms can be narrowed with a collimator (a plate with holes of definite depth-to-diameter ratio) that is placed between the target and substrate [1]. A disadvantage of this method is that the collimator decreases the deposition rate, which, in addition, varies with time because of the shrinking of the holes due to the metal deposition on their walls. Moreover, this technique fails to provide a high-quality metal coating for structures with opening diameters less than 0.25 μm and aspect ratios larger than 3.

This problem can be resolved by ionizing the sputtered metal atoms because the motion of the produced ions can be controlled by the external magnetic field or the electric field in the sheath near the substrate.

One of the possible methods for ionizing metal atoms is to combine a magnetron source with an inductively coupled discharge source.

One- to three-turn RF antenna is placed between the magnetron and substrate. The antenna is powered at 13.56 MHz to produce an inductively coupled plasma. The atoms of the sputtered metal are ionized during their motion from the magnetron target to the substrate. The degree of ionization of the sputtered metal attains 30%, and the fraction of metal ions (whose velocities are much higher than the atom velocity) in the total flux ranges from 20% at a pressure of 5 mtorr to 80% at a pressure of 50 mtorr [2–5]. There is an optimum ratio between the powers of the magnetron discharge and the inductively coupled discharge. At high magnetron powers such that the density of the metal atoms is higher than the argon density, the quality of the metal coating decreases. Since the ionization energies of copper and aluminum are lower than that of argon, the presence of a large amount of metal atoms reduces the plasma temperature and, consequently, the ionization rate.

Another method is based on the use of a microwave electron-cyclotron resonance (ECR) discharge, in which the plasma is produced in a magnetic field due to the strong absorption of microwave radiation under the ECR conditions. In such a discharge, a plasma with a density higher than 10^{11} cm^{-3} and degree of ionization of metal atoms from 30 to 90% can be created at pressures of several mtorr [6–8].

In this paper, the spatial distributions of the xenon plasma parameters behind an aluminum target and the influence of sputtered metal atoms on these parameters are studied using probe and spectroscopy techniques. We note that metal plasma is difficult to investigate because the probe measurements are hampered by coating the probe insulator with metal, whereas the optical methods for measuring the electron temperature and atom density do not provide good accuracy.

2. EXPERIMENTAL SETUP AND DIAGNOSTIC TECHNIQUES

We carried out experiments on the sputtering of an aluminum target in a plasma source based on a microwave ECR discharge in a hybrid magnetic field. A schematic of the experimental facility is shown in Fig. 1. A detailed description of it is given in [9]. The vacuum chamber consists of a plasma source (15 cm in diameter and 25 cm long) and a reactor (35 cm diameter and 60 cm long). The working gas is xenon. The magnetic field is produced by three electromagnets and twelve

1063-780X/01/2707-0625$21.00

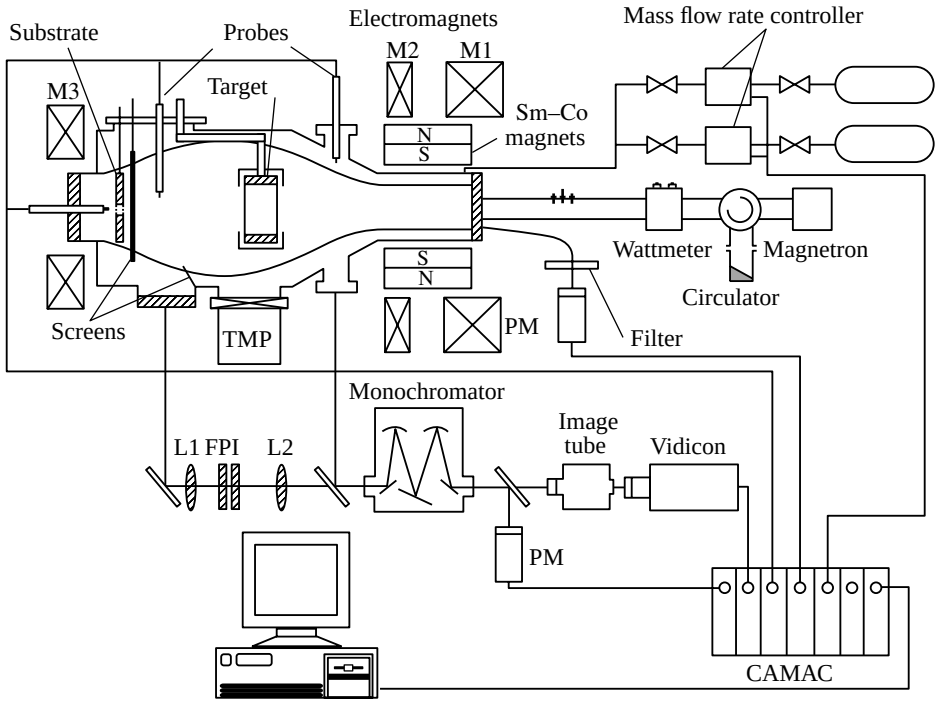

Fig. 1. Schematic of the experimental apparatus.

permanent Sm–Co magnets. The axial profile of the magnetic field at a current of 210 A is shown in Fig. 2. This profile allowed us to produce a plasma with a density higher than 10^{11} cm^{-3} at a distance of 40 cm from the source. A hollow 5-cm-long aluminum cylinder with an inner diameter of 8 cm served as a target. The cylinder was enclosed by an insulated stainless steel shield and was placed at a distance of 15 cm from the source (40 cm from the quartz window through which the microwave power was supplied). The incident, absorbed, and reflected powers were measured using a wattmeter. Coating the entrance window with a sputtered metal over ten hours of device operation only slightly affected the reflected power. The power supplied to the target was varied within the 200–400 W range. A 120-mm-diameter quartz substrate with a 7-mm-hole for fixing a probe was placed at a distance of 20 cm from the target. The third electromagnet was set in such a way that its magnetic field lines were normal to the substrate.

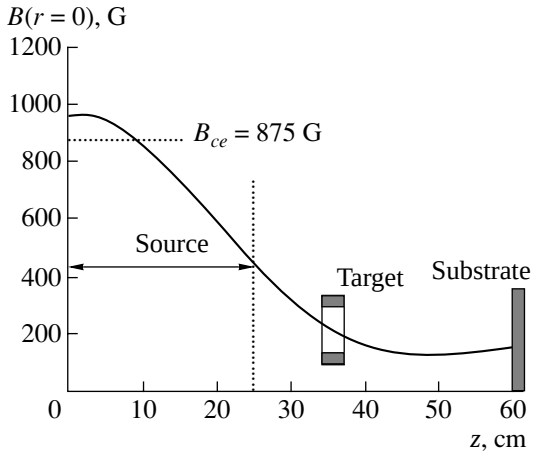

Fig. 2. Magnetic field produced by the electromagnets at I_{magn} = 210 A and r = 0 cm.

The efficiency of ionization of metal atoms depends on the atom and electron densities, electron energy, and the presence of metastable atoms of the plasma-forming gas. The electron temperature, electron energy distribution function, ion density, floating probe potential, and plasma potential were determined from probe measurements. Most of the measurements were taken with cylindrical probes because they are less sensitive to metal dusting. The probe tip was made of a tungsten wire 0.35 mm in diameter and 6 mm long. To reduce the influence of the magnetic field, the probe tip was set normal to the magnetic field lines. The probe tip was encased in ceramic (0.6 mm i.d.) and quartz (5 mm i.d.) tubes to prevent an electric short circuit. Before measuring the current–voltage (I–V) characteristic, a voltage of –80 V was applied to the probe in order to clean it by ion bombardment. A 3-mm-diameter disc-shaped plane probe was used to measure the ion density at the

discharge axis. The magnetic field in the measurement region behind the target was less than 150 G.

The *I–V* characteristics were recorded with the help of CAMAC modules and a special computer code. The recording system consisted of a digital-to-analog converter, a voltage amplifier (with an output voltage range from –80 to +80 V at an output current of up to 500 mA and a voltage rise time of up to 10 V/μs), a measurement unit, an analog multiplexer, and an analog-to-digital converter (f = 1 MHz). The probe *I–V* data included up to 640 points (voltage–current pairs, each of them being an average over ten measurements) and was recorded in a time less than 5 s. A built-in graphic program permitted us to monitor and select the data obtained.

The *I–V* data obtained were smoothed with cubic splines; then, the first and second derivatives of the probe current were calculated to determine the plasma potential V_s and the electron energy distribution function (EEDF) $f(E)$, respectively. The electron temperature T_e was determined from the slope of the logarithm of the probe electron current versus voltage to the left of the plasma potential.

Without sputtering, the plasma density was determined from the ion saturation current using the technique proposed in [10]. However, the ion saturation current of a cylindrical probe changes due to formation of a sheath. In this case, the ion current was determined by the formula $I_{Xe^+} = en_{Xe^+}S(kT_e/2\pi M_{Xe})^{1/2}i_i$, where M_{Xe} is the xenon ion mass, S is the probe area, e is the electron charge, k is the Boltzmann constant, and T_e is the electron temperature. The values of the correction coefficient i_i, which depends on the r/λ_D ratio (where λ_D is the Debye radius), and the dimensionless potential $X = e(V_s - V_p)/kT_e$ (where V_s and V_p are the plasma and probe potentials, respectively) were taken from [10]. The obtained density values agree within a 30% accuracy with those derived from the ion saturation current of a plane probe by the formula $I_{Xe^+} = 0.61en_{Xe^+}S(kT_{e1}/M_{Xe})^{1/2}$.

With sputtering, the probe also collects metal ions. Hence, taking into account the Bohm formula for the ion velocity, the ion current to a plane probe is

$$I_{Xe^+ + Al^+} = 0.61eS\left(\frac{n_{Al^+}}{\sqrt{M_{Al}}} + \frac{n_{Xe^+}}{\sqrt{M_{Xe}}}\right)\sqrt{kT_{e2}},$$

where n_{Al^+} is the density of Al ions. This formula was used to estimate the value of n_{Al^+} from the difference between the ion currents with and without target sputtering. The measurements show that the electron temperature T_{e2} and the intensity of the Xe ion emission decrease by several percent on applying the voltage to the target. Assuming that the Xe ion density does not change, the difference between the ion currents in the discharge with and without applying the voltage to the target is equal to the Al ion current. The density of Al ions was calculated by the formula

$$n_{Al^+} = n_{Xe^+}\sqrt{\frac{M_{Al}T_{e1}}{M_{Xe}T_{e2}}}\left(\frac{I_{Xe^+ + Al^+} - I_{Xe^+}}{I_{Xe^+}} + 1 - \sqrt{\frac{T_{e2}}{T_{e1}}}\right).$$

Due to the influence of the magnetic field, the electron density n_e determined from the electron current at the probe under the plasma potential is lower by a factor of 2.5–3. On the other hand, the value of n_{Al^+} can also be estimated from the ratio between the electron densities measured with and without applying voltage to the target.

The plasma emission spectra were studied with the help of a monochromator. The emission could be observed from the regions located at a distance of 10 cm in front of the target and 10–20 cm behind the target and also through the source entrance window using an optical fiber (Fig. 1). The atom and electron temperatures were determined using a Fabry–Perot interferometer (FPI), which was placed in front of the monochromator. A vidicon with an electron-optical converter was used as a detector.

3. RESULTS AND DISCUSSION

Measurements were carried out in xenon plasma at electromagnet currents of 210 A, which corresponded to a magnetic field induction of B_w = 960 G near the quartz window. It was shown in [11] that, within an 8-cm-diameter region where the target was situated, the discharge plasma in such a field was rather dense, but spatial variations in the plasma density attained 40%.

Figure 3 presents the ion current (squares) measured by a probe located at a distance of 12 cm from the target in the center of the discharge and the target current (circles) as functions of the microwave power. The ion current increases proportionally to the microwave power and does not saturate at high powers. The target current I_{targ} and the intensity J of the Al 396.1-nm spectral line versus the target voltage U_{targ} are shown in Fig. 4. The rapid increase in the target current is followed by its saturation at $U_{targ} > 200$ V. The intensity of Al line emission increases linearly until U_{targ} = 500 V; then, the growth rate decreases. Such a dependence is explained by the fact that the metal sputtering yield increases within the 100–500 V voltage range.

The current–voltage characteristics measured with a plane probe located at the chamber axis behind the Al target, at a distance of 15 cm from it, with and without target sputtering are shown in Fig. 5. The characteristics are easily reproducible. The ion (see the inset in Fig. 5) and electron currents are seen to increase on applying the voltage to the target. Note that the average density of the target ion current is approximately half of

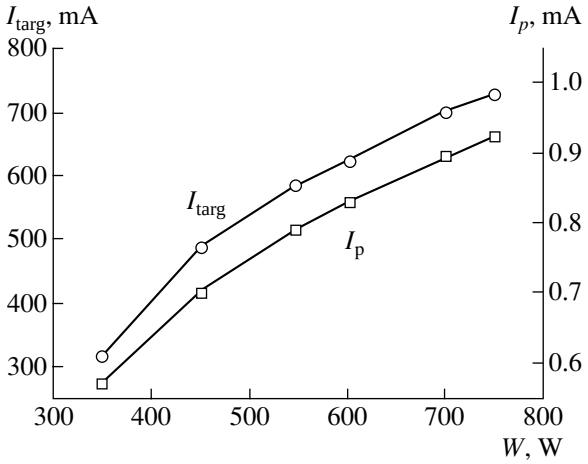

Fig. 3. Target current and saturation ion current of a plane probe vs. absorbed microwave power for p = 2.4 mtorr, 30-sccm flow rate, and U_{targ} = 500 V.

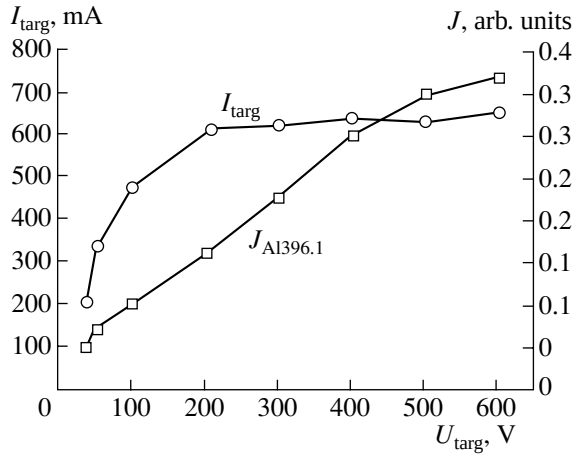

Fig. 4. Target current and the intensity of the Al 396.1-nm spectral line vs. target voltage for p = 2.4 mtorr, 30-sccm flow rate, and W_{abs} = 600 W.

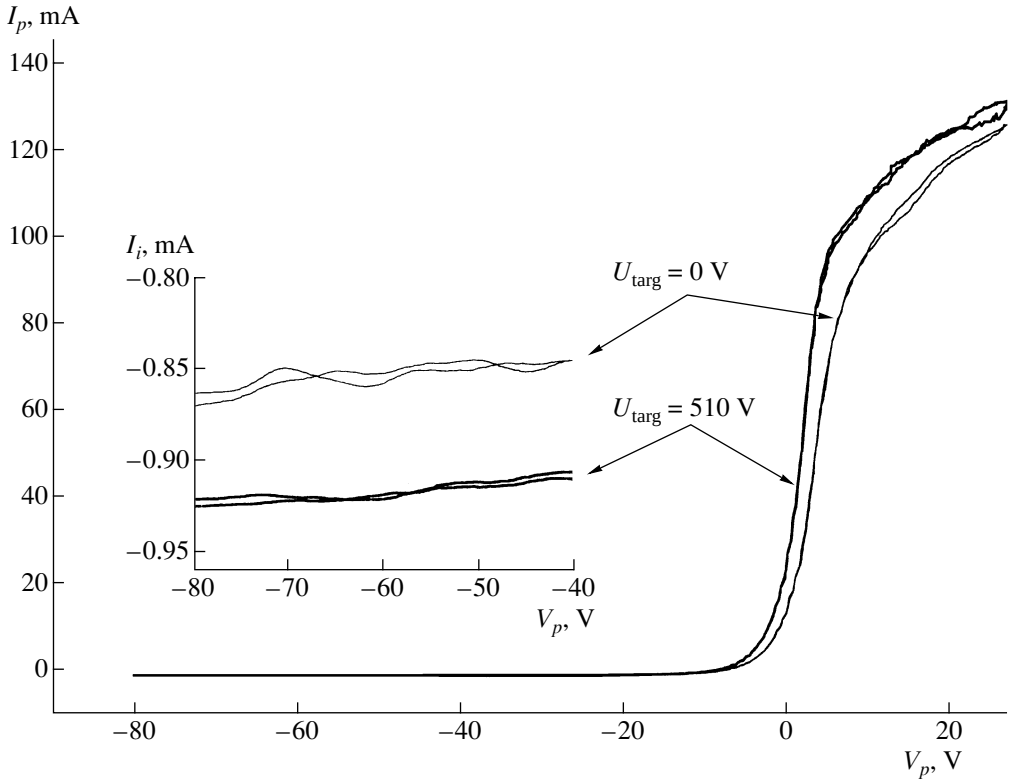

Fig. 5. Current–voltage characteristics of a probe placed at a distance of 15 cm from the Al target with (heavy curves) and without (light curves) sputtering for p = 2.4 mtorr, 30-sccm flow rate, W_{abs} = 750 W, U_{targ} = 510 V, I_{targ} = 725 mA, $n_{Xe^+} = 6.3 \times 10^{11}$ cm^{-3}, and $n_{Al^+} = 3 \times 10^{10}$ cm^{-3}.

the probe ion current. The erosion of the target indicates that the current is distributed nonuniformly over the target, being higher at its forepart. In addition, the plasma density at the chamber axis is higher than at r = 4 cm, where the target is located. The density n_{Xe^+} derived from the ion current without applying the voltage to the target is 6.3×10^{11} cm^{-3}. The density of aluminum ions n_{Al^+} derived from the difference between the ion currents using the procedure described

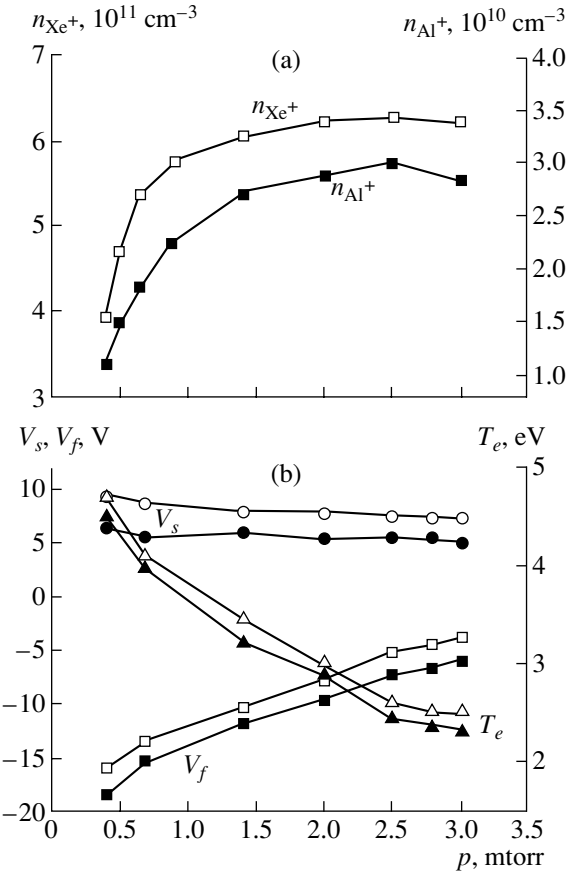

Fig. 6. Pressure dependences of (a) xenon and aluminum ion densities and (b) the plasma potential V_s, floating potential V_f, and electron temperature T_e 15 cm behind the target for W_{abs} = 700 W and W_{targ} = (open symbols) 0 and (closed symbols) 360 W.

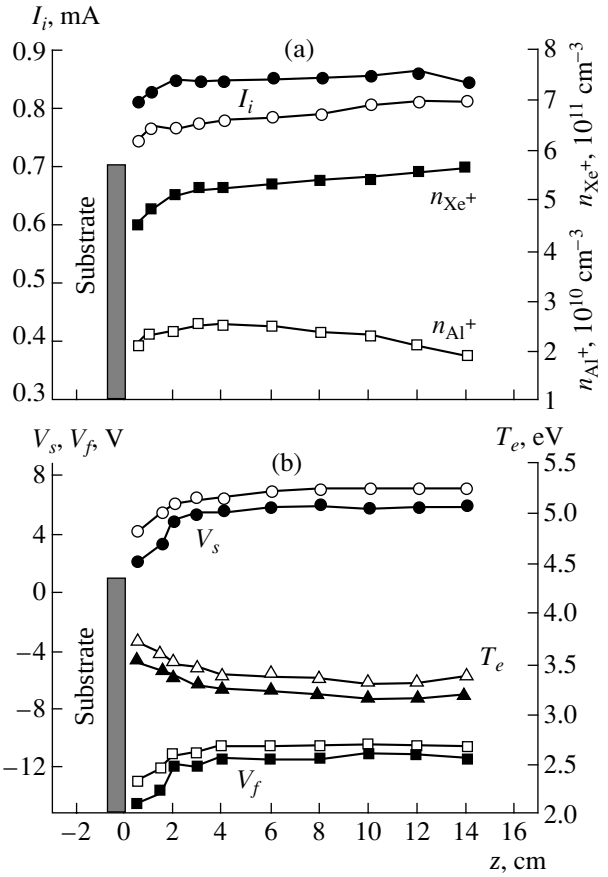

Fig. 7. Axial profiles (behind the target) of (a) the ion current I_i and xenon and aluminum ion densities and (b) the plasma potential V_s, floating potential V_f, and electron temperature T_e for p = 1.6 mtorr, 20-sccm flow rate, W_{abs} = 650 W, and W_{targ} = (open symbols) 0 and (closed symbols) 330 W.

above is 3×10^{10} cm^{-3}. On applying the voltage, the electron temperature changes only slightly (from 2.6 to 2.5 eV).

The pressure dependences of the discharge parameters behind the target, at a distance of 15 cm from it, are shown in Fig. 6. It is seen that the xenon ion density reaches its maximum at a pressure of 2.5 mtorr and then decreases. Note that the xenon ion density in this region is determined mainly by the plasma flow from the source, rather than local ionization. The ionization rate in the source is proportional to the pressure and the ionization rate constant, which depends on the ionization cross section and electron energy distribution function. At low pressures, the plasma density decreases due to the low density of neutral atoms; at high pressures, it decreases due to the decrease in the electron temperature. Downstream from the source, the plasma density profile is affected by ion–neutral collisions. As a result, the maximum plasma densities in the source and reactor are attained at different pressures [11]. In contrast, the Al ion density is determined by local ionization. The mean free path for the ionization of aluminum ions is equal to $\lambda_i = u_{Al}/\langle\sigma_i v_e\rangle n_e$, where u_{Al} is the velocity of sputtered aluminum atoms, $n_e\langle\sigma_i v_e\rangle = \int_{E_i}^{\infty} v\sigma_i f(E)dE$, σ_i is the ionization cross section, and E_i is the ionization energy. As the pressure increases, the velocity of sputtered Al atoms decreases due to collisions with Xe atoms (thermalization effect), which compensates for the decrease in the electron temperature. Furthermore, the increase in the pressure increases the probability of Al ionization due to nonresonant charge transfer.

Both the plasma potential and the absolute value of the floating potential (Fig. 6b) decrease with pressure because of a decrease in the number of high-energy electrons. When the voltage is applied to the target, the electron temperature decreases by only several percent because the metal ion density is no higher than 10% of the xenon ion at the given sputtering powers.

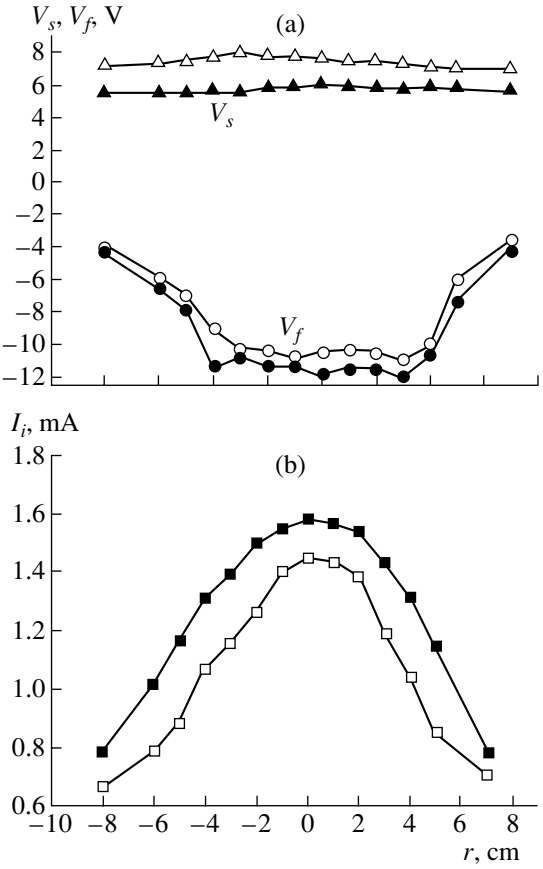

Fig. 8. Radial profiles of (a) the plasma and floating potentials and (b) the ion current I_i behind the target (at a distance of 15 cm from it) with (closed symbols) and without (open symbols) sputtering (cylindrical probe, p = 1.6 mtorr, 20-sccm flow rate, W_{abs} = 650 W, and W_{targ} = 330 W).

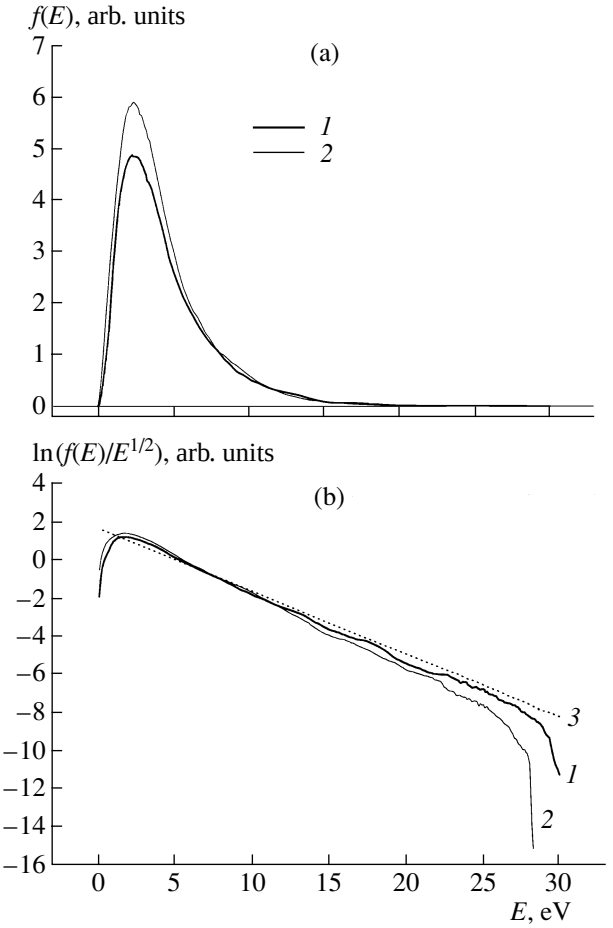

Fig. 9. (a) EEDF and (b) EEPF 15 cm behind the target at p = 2.4 mtorr, 30-sccm flow rate, W_{abs} = 730 W, and W_{targ} = 360 W for (*1*) U_{targ} = 0 V and E_{mean} = 4.5 eV and (*2*) U_{targ} = 510 V and E_{mean} = 4.3 eV. Curve *3* shows the EEPF for a Maxwellian distribution and E_{mean} = 4.5 eV.

Figure 7a shows the ion currents versus the distance from the substrate with (closed circles) and without (open circles) sputtering. The target is at a distance of 20 cm from the substrate. It can be seen that the difference between these currents and the Al ion density both increase with distance. This is obvious because ionization probability increases with the path length. The xenon density slightly decreases with distance from the target. Figure 7b shows the plasma potential V_s, floating potential V_f, and electron temperature versus the distance from the substrate. On applying the voltage to the target, the plasma potential V_s decreases by 1–2 V, the floating potential V_f becomes more negative, and both the difference $V_s - V_f$ and T_e slightly decrease. It is known that, when the electron energy distribution is Maxwellian, the difference $V_s - V_f$ and T_e are related by the formula $V_s - V_f = (T_e/2)\ln(I_{es}/I_{is})$, where I_{es} and I_{is} are the electron and ion saturation currents. Under the given conditions, the electron temperature T_e derived from this formula is lower than that determined from the *V–I* characteristic, because the magnetic field suppresses the electron current. Note that the low value of the plasma potential is explained by the fact that the plasma is confined in the transverse direction by the magnetic field and in the longitudinal direction by the electric field of the substrate, which is at the floating potential. The plasma potential, which depends slightly on the radius, decreases from 8.5 to 6 V on applying the voltage to the target (Fig. 8a). The floating potential V_f is negative and depends on the radius. The difference $V_s - V_f$ reaches its maximum (19 V) inside the target ($|r| < 4$ cm), where the high-energy electrons are located. At the periphery, the difference $V_s - V_f$ falls to 11–12 V. Figure 8b shows the radial profiles of the ion current at a distance of 15 cm from the target. Within the 8-cm-diameter region, the radial drop in the ion current changes from 40 to 20% when the sputtering voltage is turned on.

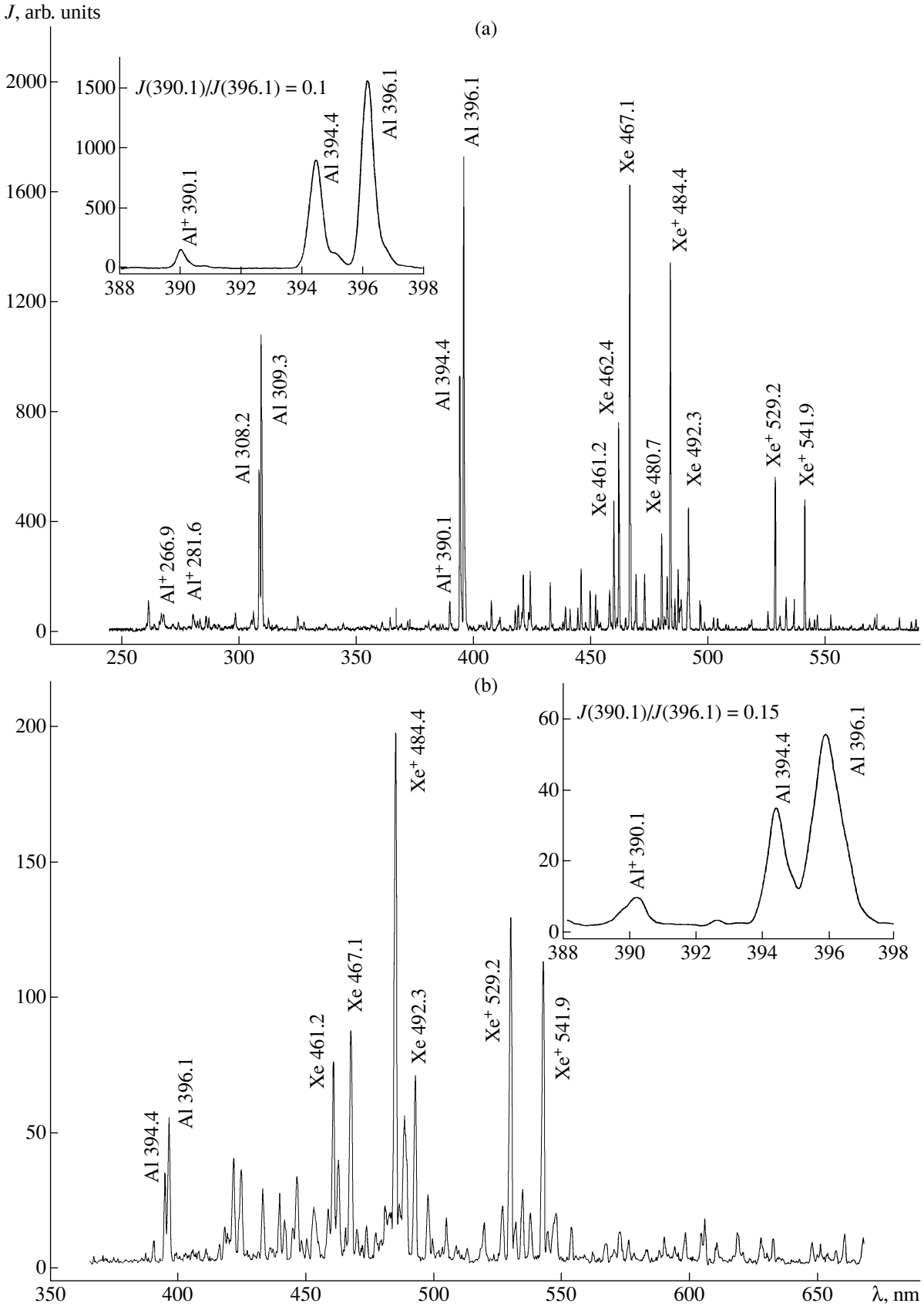

Fig. 10. Emission spectrum of the plasma (a) 15 cm behind the target and (b) in the source for p = 1.6 mtorr, 20-sccm flow rate, W_{abs} = 750 W, and W_{targ} = 360 W.

Figure 9a presents the nonnormalized EEDF $f(E)$. The area below the curve is proportional to the electron density. When the voltage U_{targ} is applied to the target, this area increases by 10%. The distribution function increases mainly in the low-energy region, and the mean electron energy $E_{\text{mean}} = \frac{1}{n_e} \int_0^\infty f(E) E dE$ changes only slightly (from 4.5 eV at $U_{\text{targ}} = 0$ to 4.3 eV at $U_{\text{targ}} =$ 510 V). The electron energy probability functions (EEPF) obtained by dividing $f(E)$ from Fig. 9a by $\sqrt{E}$ [12] are shown in Fig. 9b on the logarithmic scale. For comparison, the figure also shows an analogous probability function for a Maxwellian electron energy distribution. This function is convenient because, for a Maxwellian distribution, its logarithm depends linearly on the electron energy. Due to inelastic collisions with atoms and ions, the number of electrons with energies higher than 10 eV is depleted as compared to a Maxwellian distribution. Moreover, with the sputtering power turned on, the high-energy tail of the EEDF decreases more rapidly. This is related to the presence of metal atoms in the discharge. The excitation and ionization energies of Al (~3 and 5.98 eV, respectively) are lower than those of Xe (~10 and 12.13 eV, respectively), whereas the cross sections for electron-impact excitation and ionization of Al are higher than those of Xe. As a result, the number of high-energy electrons and the line emission intensities of Xe atoms and ions decrease. Furthermore, the difference between the plasma potential V_s and the substrate floating potential V_f can be regarded as a potential barrier through which only electrons with sufficiently high energies can pass. Due to plasma quasineutrality, the value of this barrier is established at such a level that the electron and ion fluxes toward the substrate balance each other. When the number of high-energy electrons that are able to overcome this barrier decreases, the balance between the electron and ion fluxes is violated. In order for the electron flux to increase, the difference $V_s - V_f$ should decrease, as is observed in the experiment.

The plasma emission spectrum behind the target is shown in Fig. 10a. As the distance from the target increases from 5 to 17 cm, the ratio between the intensities of the Al^+ 390.1-nm and Al 396.1-nm lines increases from 0.02 to 0.1. For reference, Fig. 10b shows the plasma emission spectrum in the source. It is seen that the ion lines are dominating, which indicates a high degree of Xe ionization. The relative intensities of the Al lines decrease as the distance from the target increases. However, the ratio between the intensities of the Al^+ 390.1-nm and Al 396.1-nm lines increases. Thus, the degree of ionization increases with distance both upstream and downstream from the target.

Now, we make some estimates that cannot be considered completely accurate because of the large scatter in the data available in the literature. Nevertheless, they provide a good idea of the order of magnitude of the estimated values. According to measurements [13], the most probable energy of sputtered Al atoms is $E_{\text{prob}} =$ 3 eV, which corresponds to the velocity $u_{\text{Al}} = 4.6 \times 10^5$ cm/s. Taking the value of σ_i from [4] and the values $n_e = 6.3 \times 10^{11}$ cm^{-3} and $T_e = 2.5$ eV measured at $p =$ 2.5 mtorr, we obtain that the mean free path with respect to ionization is $\lambda_i \approx 105$ cm. Then, according to the formula $n_{\text{Al}^+}/n_{\text{Al}} = 1 - \exp(-z/\lambda_i)$, about 13% of Al atoms will be ionized over the path length $z = 15$ cm. Using the above value $n_{\text{Al}^+} = 3 \times 10^{10}$ cm^{-3}, we obtain that the Al atom density is $n_{\text{Al}} = 2 \times 10^{11}$ cm^{-3}.

The rate of metal film deposition depends on the atom and ion fluxes. The flux of Al ions is $\Gamma_{\text{Al}^+} = 0.61 n_{\text{Al}^+} u_{\text{Al}^+}$. The velocity of ions arriving at the substrate is determined by the Bohm formula $u_{\text{Al}^+} = (kT_e/M_{\text{Al}})^{1/2} = 2.95 \times 10^5$ cm/s; hence, $\Gamma_{\text{Al}^+} = 5.5 \times 10^{15}$ cm^{-2} s^{-1}. The flux of Al atoms is $\Gamma_{\text{Al}} = 0.25 n_{\text{Al}} u_{\text{Al}}$. The atom and ion temperatures were determined using an FPI and a vidicon as a detector (Fig. 1). The measured temperatures of Xe atoms and ions were 0.05 and 0.4 eV, respectively. The temperature of Al atoms was not measured. At the given pressure, the mean free path of Al atoms between collisions with Xe atoms is equal to 3.5 cm. At a distance of 15 cm from the target, the most probable energy of Al atoms after four collisions is $(1 - q)^4 E_{\text{prob}} = 0.11$ eV, where $q = 4M_{\text{Al}}M_{\text{Xe}}/(M_{\text{Al}} + M_{\text{Xe}})^2$ is the energy fraction lost by an Al atom per collision. Then, we have $u_{\text{Al}} = 0.9 \times 10^5$ cm/s; the flux $\Gamma_{\text{Al}} \approx 4.5 \times 10^{15}$ cm^{-2} s^{-1}; and the relative contribution of ions to the total flux, $\Gamma_{\text{Al}^+}/(\Gamma_{\text{Al}^+} + \Gamma_{\text{Al}})$, is 55%.

4. CONCLUSION

The spatial distribution of the degree of ionization of metal sputtered with a microwave ECR discharge has been studied using the probe and optical emission spectroscopy techniques. The study is aimed at developing a system for the metallization of submicron ULSI structures.

ACKNOWLEDGMENTS

This study was supported by the Ministry of Education of the Russian Federation (under the program "Critical Technologies").

REFERENCES

1. S. M. Rossnagel, Thin Solid Films **263**, 1 (1995).
2. J. Hopwood and F. Qian, J. Appl. Phys. **78**, 758 (1995).
3. C. A. Nickols, S. M. Rossnagel, and S. Hamaguchi, J. Vac. Sci. Technol. B **14**, 3270 (1996).

4. M. Dickson and J. Hopwood, J. Vac. Sci. Technol. A **15**, 2307 (1997).
5. S. Shibuki, H. Kanao, and T. Akahori, J. Vac. Sci. Technol. B **15**, 60 (1997).
6. S. Takehiro, N. Yamanaka, H. Shindo, *et al.*, Jpn. J. Appl. Phys. **30**, 3657 (1991).
7. W. M. Holberg, J. S. Logan, H. J. Grabarz, *et al.*, J. Vac. Sci. Technol. A **11**, 2903 (1993).
8. S. M. Gorbatkin, D. B. Poker, C. Doughty, *et al.*, J. Vac. Sci. Technol. B **14**, 1853 (1996).
9. N. P. Poluektov and Yu. P. Tsar'gorodtsev, Prib. Tekh. Éksp., No. 4, 150 (1996) [Instrum. Exper. Techniques **39**, 611 (1996)].
10. C. Steinbruchel, J. Vac. Sci. Technol. A **8**, 1663 (1990).
11. N. P. Poluektov, Yu. P. Tsar'gorodtsev, and I. G. Usatov, Fiz. Plazmy **25**, 981 (1999) [Plasma Phys. Rep. **25**, 905 (1999)].
12. M. A. Lieberman and A. J. Lichtenberg, in *Principles of Plasma Discharges and Materials Processing* (Wiley, New York, 1994), p. 177.
13. R. V. Stuart, G. K. Wenher, and G. S. Anderson, J. Appl. Phys. **40**, 803 (1969).

Translated by N. N. Ustinovskiĭ